Development of novel paullone-based PROTACs as anticancer agents

Srinivas Manda [a,b,*], Vamsee Krishna Chatakonda [a], Vinod G. Ugale [c] , Shalini Tanwar [a], Chandana Raperthi [a], Maheshkumar Borkar [d], Poonam Eknath Nale [a], Srinivas Pasikanti [a], Pedavenkatagari Narayana Reddy [b,*]

[a] Aurigene Pharmaceutical Services Limited, Miyapur, Hyderabad, Telangana 500090, India
[b] Department of Chemistry, School of Science, Gitam Deemed to be University, Hyderabad, Telangana 502329, India
[c] Department of Pharmaceutical Chemistry, R. C. Patel Institute of Pharmaceutical Education and Research, Shirpur 425405, Maharashtra, India
[d] Deparment of Pharmaceutical Chemistry, SVKM's Dr. Bhanuben Nanavati College of Pharmacy, Mumbai, Maharashtra 400056, India

ARTICLE INFO

ABSTRACT

Proteolysis-targeting chimera (PROTACs) represents a promising modality that has gained significant attention for cancer treatment. Using PROTAC technology, we synthesized novel structurally modified paullone-based PROTACs using Cereblon (CRBN) and Von Hippel–Lindau (VHL) E3 ligands. Compared with standard Doxorubicin, PROTAC **23a** significantly inhibited the growth of MCF-7 breast cancer cells ($IC_{50} = 0.10$ μM) and A549 lung cancer cells ($IC_{50} = 0.12$ μM). The degradation efficiency of these new PROTACs was assessed by immunoblotting assays in MCF-7 cells. Western blotting results revealed that PROTAC **23a** degrades cyclin-dependent kinase 1 (CDK1) at concentrations ranging from 5.5 to 16 μM, leading to anticancer effects. Molecular docking was used to confirm the affinity of active PROTAC **23a** for the CDK1 binding site. Our findings demonstrated the importance of paullone-based PROTACs as CDK1 degraders, which might be exploited to identify more effective clinical candidates for breast and lung cancer treatment.

1. Introduction

Cancer is the second most significant cause of death worldwide, accounting for roughly one out of every six deaths [1]. Despite breakthroughs in cancer detection and therapy, the prognosis remains poor due to the evolution of drug resistance, indicating the need for new therapeutic regimens for effective disease management [2–14]. Cell cycle dysregulation is a hallmark of malignancies, resulting in dysregulated cell proliferation and, eventually, tumour development [15]. Cyclin-dependent kinases (CDKs) that promote transition through the cell cycle were attractive targets for the development of cancer therapeutics [16–19]. CDKs play a key role in the progression of the cell cycle through its four distinct phases (G1, S, G2 and M) is dependent on the integration of extra- and intracellular signals [20,21]. Several selective inhibitors or pan-inhibitors of CDK have been produced over the past decades [22–28]. In particular, CDK1 emerged as a key determinant of

mitotic progression. The entry into mitosis is controlled by the cyclin B/CDK1 complex [29]. Furthermore, CDK1 over expression has been detected in breast cancer, esophageal adenocarcinoma, gastric cancer, ovarian cancer, and liver cancer [30]. CDK1 dysregulation in cancer is more relevant than other kinases since it is the universal master kinase that has been conserved from yeast to humans. CDK1 deregulation leads to aggressive tumour growth, genomic instability, and increased cell proliferation [31]. Inhibition of the expression and activation of CDK1 effectively suppresses oncogenic cell function in many cancer types. As a result, there is an urgent need to identify therapeutic drugs that selectively target CDK1 in cancer cells.

PROTAC technology has been employed in recent years to stimulate protein degradation by targeting specific sites with connected small molecules [32]. Over the last decade, the use of a PROTAC method has reduced medication resistance [33] and improved the prognosis of cancer patients [34]. PROTAC has various advantages over traditional

Fig. 1. PROTAC induced degradation and rationally designed paullone PROTACs.

pharmaceuticals, including the ability to degrade non-druggable targets without requiring binding to the target protein's active region to exert its effects. Despite advances in PROTAC technology [35–39], the synthesis of PROTACs still represents a significant burden and new synthetic methodologies are needed. Targeting CDK1 using the PROTAC strategy is a promising approach, given the role of CDK1 in cancer [40].

Paullones (7,12-dihydro-5*H*-indolo[3,2-*d*][1]benzazepin-6-one) a group of ATP-competitive represent a class of small molecule CDK1 inhibitors [41,42]. Several paullone analogues have been designed and synthesized, hoping to develop more efficient anticancer drugs with either improved CDK targeting or binding affinity [43–49]. Notably, small molecule paullone derivatives targeting CDK1 have already been studied [50,51]. However targeting CDK1 using the paullone-based PROTACs is not reported. Thus, for cancer treatment, we aimed to develop paullone-based PROTACs that target CDK1 with significantly greater specificity than the original CDK1 inhibitors.

2. Rational design

PROTACs comprise of three essential components the ligand for the target protein, the ligand for the E3 ligase, and the linker that connects these two components. These hetero bifunctional molecules bind to an E3 ligase and target protein of interest (POI), to form a ternary complex that leads to target ubiquitination and subsequent proteasomal degradation (Fig. 1) [52]. To our knowledge, no report has been published on the development of paullone based PROTACs targeting the CDK1 protein. This study, used CRBN and VHL E3 ligands because both have been widely adopted in various PROTACs [53–57]. PROTACs were designed by connecting paullone with CRBN and VHL ligands through various linkers (Fig. 1). Linkers of different lengths and chemical nature such as linear aliphatic and polyethylene glycol chains and aromatic substituted polyethylene glycol chains have been investigated.

3. Materials and methods

3.1. Chemistry

All reactions were carried out under an argon atmosphere with dehydrated solvents under anhydrous conditions unless otherwise noted. Reagents were obtained from commercial suppliers unless otherwise noted. All the heating reactions were carried out by using an oil bath. Reactions were monitored by thin-layer chromatography (TLC) carried out on silica gel 70 F254 glass plates (Wako; 0.25 mm thickness) with visualization by UV light (254 nm) or by staining with *p*-anisaldehyde or phosphomolybdic acid. Column chromatography was

performed on Teledyne combi flash isco chromatograph Chromatorex PSQ 100B (Fuji Silysia; Redisef, spherical, neutral, 40–63 μm, 100 μm). High-performance liquid chromatography (HPLC) was performed on a JASCO PU-2089 Plus quaternary gradient pump with a JASCO UV-2075 Plus Intelligent UV/VIS detector using a Kinetex 5u C18 100A AXIA column (5 μm, 250 mm × 21.2 mm). The flow rate for HPLC was 8.0 mL/min with 70 % MeCN/H$_2$O. UV detection was performed at 366 nm.

3.1.1. General procedure for the synthesis of PROTACs 14a-e

To a stirred solution of 6-oxo-5,6,7,12-tetrahydrobenzo[2,3]azepino [4,5-*b*]indole-9-carboxylic acid **8** (1.1 eq) in dimethylformamide (DMF) (5.0 mL) were added hexafluorophosphate azabenzotriazole tetramethyl uranium (HATU) (1.5 eq), *N,N*-diisopropylethylamine (DIPEA) (6.0 eq) and **13a-e** (1.0 eq). Then the resulting reaction mixture was stirred at RT for 12 h. Progress of the reaction was monitored by TLC. After completion of reaction the reaction mixture was diluted with chilled water (50 mL). The precipitated solid was filtered and washed with water (20 mL), dried under reduced pressure to get a crude compound. The obtained crude was purified by combiflash chromatography (4 g silica gel column; gradient elusion 6 % MeOH in DCM) to afford the desired PROTACs **14a-e**.

3.1.2. N-(7-((2-(2,6-dioxopiperidin-3-yl)-1,3-dioxoisoindolin-4-yl) amino)-7-oxoheptyl)-6-oxo-5,6,7,12-tetrahydrobenzo[2,3]azepino[4,5-b] indole-9-carboxamide (14a)

Yield: 20 %; ^{1}H NMR (400 MHz, DMSO-d_6, ppm): δ 11.84 (s, 1H), 11.16 (s, 1H), 10.15 (s, 1H), 9.72 (s, 1H), 8.49–8.45 (m, 1H), 8.40–8.37 (m, 1H), 8.26 (bs, 1H), 7.82 (t, *J* = 7.6 Hz,1H), 7.76–7.70 (m, 2H), 7.61–7.59 (m, 1H), 7.45–7.37 (m, 2H), 7.31–7.25 (m, 2H), 5.16–5.12 (m, 1H), 3.54 (s, 2H), 3.32–3.24 (m, 3H), 2.89–2.85 (m, 1H), 2.67–2.57 (m, 2H), 2.48–2.46 (m, 1H), 2.08–2.04 (m, 1H), 1.65–1.55 (m, 4H), 1.39–1.23 (m, 4H); ^{13}C NMR (100 MHz, CDCl$_3$, ppm): δ 172.87, 172.13, 171.76, 171.62, 171.54, 169.89, 167.97, 167.71, 167.56, 166.87, 166.75, 138.95, 138.85, 138.72, 136.57, 136.16, 133.71, 133.61, 131.50, 128.38, 126.95, 126.44, 125.99, 125.87, 123.84, 122.59, 122.41, 121.91, 118.38, 117.48, 117.12, 111.01, 108.46, 48.94, 31.68, 30.97, 29.24, 28.40, 26.39, 24.84, 22.03; LCMS: *m/z* = 675.30 [M+H]$^+$; HR-ESIMS: *m/z*: 674.9773 calcd for C$_{37}$H$_{34}$N$_6$O$_7$+H$^+$ (674.7140); HPLC purity 95.66 %.

3.1.3. N-(10-((2-(2,6-dioxopiperidin-3-yl)-1,3-dioxoisoindolin-4-yl) amino)-10-oxodecyl)-6-oxo-5,6,7,12-tetrahydrobenzo[2,3]azepino[4,5-b] indole-9-carboxamide (14b)

Yield: 16.6 %; ^{1}H NMR (400 MHz, DMSO-d_6, ppm): δ 11.83 (s, 1H), 11.16 (s, 1H), 10.15 (s, 1H), 9.69 (s, 1H), 8.46 (d, *J* = 8.40 Hz, 1H), 8.37

(t, J = 5.6 Hz, 1H), 8.26–8.23 (m, 1H), 7.82 (t, J = 5.6 Hz, 1H), 7.76–7.70 (m, 2H), 7.60 (d, J = 7.6 Hz, 1H), 7.44 (d, J = 8.4 Hz, 1H), 7.41–7.37 (m, 1H), 7.30–7.25 (m, 2H), 5.17–5.12 (m, 1H), 3.54 (s, 2H), 3.30–3.25 (m, 2H), 2.90–2.85 (m, 1H), 2.67–2.57 (m, 2H), 2.47–2.33 (m, 3H), 2.08–2.04 (m, 1H), 1.63–1.53 (m, 4H), 1.31 (bs, 9H); ^{13}C NMR (400 MHz, DMSO-d_6, ppm): δ 172.82, 172.06, 171.55, 169.849, 166.71, 136.11, 135.55, 136.65, 128.29, 126.91, 126.34, 125.95, 122.53, 122.35, 121.88, 118.30, 117.41, 110.90, 108.40, 48.88, 40.51, 40.39, 36.51, 30.94, 29.33, 28.90, 28.81, 28.75, 28.52, 26.58, 24.81; LCMS: m/z = 717.25 [M+H]$^+$, HR-ESIMS: m/z, 716.9055 calcd for $C_{40}H_{40}N_6O_7+H^+$ (716.7950); HPLC purity 99.04 %.

3.1.4. N-(11-((2-(2,6-dioxopiperidin-3-yl)-1,3-dioxoisoindolin-4-yl) amino)-11-oxoundecyl)-6-oxo-5,6,7,12-tetrahydrobenzo[2,3]azepino[4,5-b]indole-9-carboxamide (14c)

Yield: 21.4 %; ^{1}H NMR (400 MHz, DMSO-d_6, ppm): δ 11.83 (s, 1H), 11.15 (s, 1H), 10.14 (s, 1H), 9.69 (s, 1H), 8.46 (d, J = 8.46, Hz, 1H), 8.36 (t, J = 5.20, Hz, 1H), 8.26 (bs, 1H), 7.84–7.80 (m, 1H), 7.76–7.71 (m, 2H), 7.60 (d, J = 7.60, Hz, 1H), 7.44 (d, J = 8.4 Hz, 1H), 7.39–7.37 (m, 1H), 7.30–7.25 (m, 2H), 5.16–5.12 (m, 1H), 3.55 (s, 2H), 3.30–3.25 (m, 2H), 2.90–2.85 (m, 1H), 2.67–2.58 (m, 2H), 2.46–2.33 (m, 3H), 2.07–2.06 (m, 1H), 1.63–1.53 (m, 4H), 1.30–1.22 (m, 11H); ^{13}C NMR (400 MHz, DMSO-d_6, ppm): δ 172.80, 172.06, 171.55, 169.78, 166.69, 136.34, 136.10, 135.55, 128.03, 126.33, 123.75, 122.40, 118.14, 117.41, 110.98, 108.50, 36.50, 30.48, 28.85, 28.53, 26.60, 24.80, 21.85; LCMS: m/z = 731.25 [M+H]$^+$; HR-ESIMS: m/z, 730.9572, calcd for $C_{41}H_{42}N_6O_7+H^+$ (730.8220); HPLC purity 98.23 %.

3.1.5. N-(12-((2-(2,6-dioxopiperidin-3-yl)-1,3-dioxoisoindolin-4-yl) amino)-12-oxododecyl)-6-oxo-5,6,7,12-tetrahydrobenzo[2,3]azepino[4,5-b]indole-9-carboxamide (14d)

Yield: 17.08 %; ^{1}H NMR (400 MHz, DMSO-d_6, ppm) δ 11.83 (s, 1H), 11.16 (s, 1H), 10.15 (s, 1H), 9.69 (s, 1H), 8.46 (d, J = 8.4 Hz, 1H), 8.37 (t, J = 5.2 Hz, 1H), 8.26 (s, 1H), 7.82 (t, J = 8.0 Hz, 1H), 7.76–7.71 (m, 2H), 7.61 (d, J = 7.2 Hz, 1H), 7.44 (d, J = 8.4 Hz, 1H), 7.41–7.37 (m, 1H), 7.30–7.25 (m, 2H), 5.17–5.12 (m, 1H), 3.55 (s, 2H), 3.31–3 0.25 (m, 2H), 2.90–2.85 (m, 1H), 2.67–2.57 (m, 2H), 2.46–2.33 (m, 3H), 2.00–2.04 (m, 1H), 1.62–1.53 (m, 4H), 1.30–1.21 (m, 13H); ^{13}C NMR (400 MHz, DMSO-d_6, ppm): δ 172.844, 172.08, 171.57, 169.86, 167.68, 166.74, 136.54, 136.13, 135.56, 126.92, 126.34, 125.85, 123.77, 122.55, 122.37, 121.89, 118.33, 117.43, 110.96, 108.40, 48.90, 40.12, 38.86, 36.51, 31.67, 30.95, 29.34, 29.03, 28.94, 28.88, 28.78, 28.53, 26.61, 24.81, 21.99; LCMS: m/z = 743.80 [M-H]$^+$; HR-ESIMS: m/z, 744.8851 calcd for $C_{42}H_{44}N_6O_7+H+$ (744.8490); HPLC purity 99.21 %.

3.1.6. N-(2-(2-(2-((2-(2,6-dioxopiperidin-3-yl)-1,3-dioxoisoindolin-4-yl) amino)-2-oxoethoxy)ethoxy)ethyl)-6-oxo-5,6,7,12-tetrahydrobenzo[2,3]azepino[4,5-b]indole-9-carboxamide (14e)

Yield: 13.5 %; ^{1}H NMR (400 MHz, DMSO-d_6, ppm) δ 11.82 (s, 1H) 11.16 (s, 1H), 10.35 (s, 1H), 10.14 (m, 1H), 8.68–8.66 (m, 1H), 8.41 (t, J = 5.6 Hz, 1H), 8.2 (s, 1H), 7.81–7.74 (m, 2H), 7.69–7.67 (m, 1H), 7.57–7.55 (m, 1H), 7.43–7.38 (m, 2H), 7.31–7.25 (m, 2H), 5.19–5.14 (m, 1H), 4.22–4.18 (m, 2H), 3.79–3.72 (m, 4H), 3.61–3.59 (m, 2H), 3.52–3.46 (m, 4H), 2.92–2.84 (m, 1H), 2.67–2.55 (m, 2H), 2.10–2.07 (m, 1H); ^{13}C NMR (400 MHz, DMSO-d_6,ppm); δ 172.82, 171.56, 169.85, 169.35, 168.21, 166.96, 138.80, 136.39, 135.89, 131.23, 128.34, 126.92, 125.92, 124.27, 123.78, 122.53, 122.37, 121.78, 118.22, 117.54, 110.93, 108.43, 70.70, 70.16, 69.50, 69.27, 48.95, 40.12, 38.86, 31.64, 30.95, 21.94; LCMS: m/z = 691.5 [M-H]$^+$; HR-ESIMS: m/z, 692.9064 calcd for $C_{36}H_{32}N_6O_9+H+$ (692.6850); HPLC purity 99.20 %.

3.1.7. General procedure for the synthesis of PROTACS (23a-b)

To a stirred solution of 6-oxo-5,6,7,12-tetrahydrobenzo[2,3]azepino [4,5-b]indole-9-carboxylic acid 8 (1.0 eq) in DMF (5.0 mL) were added HATU (1.5eq), DIPEA (3.0 eq), and 22a-b (1.0 eq). Then the resulting reaction mixture was stirred at RT for 16 h. Progress of the reaction was monitored by TLC. After completion of reaction, the reaction mixture was diluted with chilled water (35 mL). The precipitated solid was filtered and washed with water (20 mL), dried under reduced pressure. The obtained crude was purified by combiflash chromatography (4 g silica gel column; gradient elusion 6.2 % MeOH in DCM) to afford the desired PROTACS 23a-b.

3.1.8. N-(4-(2-(2-((2-(2,6-dioxopiperidin-3-yl)-1,3-dioxoisoindolin-4-yl) amino)ethoxy)ethoxy)phenyl)-6-oxo-5,6,7,12-tetrahydrobenzo[2,3] azepino[4,5-b]indole-9-carboxamide (23a)

Yield: 16.12 %; ^{1}H NMR (400 MHz, DMSO-d_6, ppm); δ 11.93 (s, 1H), 11.11 (s, 1H), 10.18 (s, 1H), 10.07 (s, 1H), 8.42 (bs, 1H), 7.83–7.76 (m, 2H), 7.69 (d, J = 8.8 Hz, 2H), 7.58 (t, J = 7.6 Hz, 1H), 7.53 −7.49 (m, 1H), 7.42–7.38 (m, 1H), 7.32–7.26 (m, 2H), 7.17 (d, J = 8.8 Hz, 1H), 7.04 (d, J = 7.2 Hz, 1H), 6.93 (d, J = 8.8 Hz, 2H), 6.66 (t, J = 6.0 Hz, 1H), 5.08–5.04 (m, 1H), 4.11–4.09 (m, 2H), 3.81–3.79 (m, 2H), 3.70–3.69 (m, 2H), 3.60 (s, 2H), 3.54–3.49 (m, 2H), 2.93–2.84 (m, 1H), 2.67–2.54 (m, 2H), 2.05–2.01 (m, 1H); ^{13}C NMR (400 MHz, DMSO-d_6, ppm): δ 172.88, 171.60, 170.16, 168.59, 165.73, 154.45, 146.42, 139.02, 136.28, 135.60, 132.21, 128.49, 127.06, 125.82, 123.79, 122.22, 121.88, 118.13, 117.51, 114.35, 111.10, 110.72, 108.55, 69.06, 67.25, 48.68, 41.69, 40.13, 39.92, 39.08, 38.87, 31.00, 22.15; LCMS: m/z = 727.3 [M+H]$^+$; HR-ESIMS: m/z, 726.9050 calcd for $C_{40}H_{34}N_6O_8+H^+$ (726.7460); HPLC purity 92.96 %.

3.1.9. N-(4-(2-(2-(2-((2-(2,6-dioxopiperidin-3-yl)-1,3-dioxoisoindolin-4-yl) amino)ethoxy)ethoxy)ethoxy)phenyl)-6-oxo-5,6,7,12-tetrahydrobenzo [2,3]azepino[4,5-b]indole-9-carboxamide (23b)

Yield: 11.5 %; ^{1}H NMR (400 MHz, DMSO-d_6 ppm); δ 11.94 (s, 1H), 11.11 (s, 1H), 10.18 (s, 1H), 10.07 (s, 1H), 8.42 (s, 1H), 7.83–7.76 (m, 2H), 7.69 (d, J = 9.2 Hz, 2H), 7.60–7.51 (m, 2H), 7.42–7.39 (m, 1H), 7.32–7.26 (m, 2H), 7.15 (d, J = 8.0 Hz, 1H), 7.04 (d, J = 7.2 Hz, 1H), 6.92 (d, J = 8.8 Hz, 2H), 6.63 (t, J = 5.6, 1H), 5.08–5.03 (m, 1H), 4.07–4.05 (m, 2H), 3.75–3.73 (m, 2H), 3.65–3.60 (m, 7H), 3.49–3.47 (m, 3H), 2.88–2.84 (m, 1H), 2.60–2.55 (m, 2H), 2.03–1.99 (m, 1H). ^{13}C NMR (400 MHz, DMSO-d_6, ppm): δ 172.90, 171.64, 170.18, 165.77, 154.49, 146.45, 136.29, 135.62, 132.76, 126.99, 125.97, 123.83, 122.52, 122.41, 122.23, 121.93, 118.05, 117.54, 114.29, 111.23, 110.72, 108.57, 69.99, 69.84, 69.13, 68.96, 67.25, 48.58, 41.71, 40.13, 38.87, 31.70, 31.01, 22.18. LCMS: 99.13 %, m/z = 771.35 (M + 1), HR-ESIMS: m/z, 77.8038 calcd for $C_{42}H_{38}N_6O_9+H^+$ (770.7990), HPLC purity 95.56 %.

3.1.10. General procedure for the synthesis of PROTACs 29a-c

To a stirred solution of 6-oxo-5,6,7,12-tetrahydrobenzo[2,3]azepino [4,5-b]indole-9-carboxylic acid (8) (1.1 eq) in DMF (5.0 mL) were added HATU (1.5eq), DIPEA (6.0eq), and (28a-c) (1.0 eq). Then the resulting reaction mixture was stirred at RT for 12–16 h. Progress of the reaction was monitored by TLC. After completion of reaction, the reaction mixture was diluted with chilled water (50 mL). The precipitated solid was filtered and washed with water (20 mL), dried under reduced pressure to get crude compound. The obtained crude was purified by combiflash chromatography (4 g silica gel column; gradient elusion 5.5 % MeOH in DCM) to afford the desired PROTACS 29a-c.

3.1.11. 7N-(7-(((S)-1-((2R,4R)-4-hydroxy-2-(((S)-1-(4-(4-methylthiazol-5-yl)phenyl)ethyl)carbamoyl)pyrrolidin-1-yl)-3,3-dimethyl-1-oxobutan-2-yl)amino)-7-oxoheptyl)-6-oxo-5,6,7,12-tetrahydrobenzo [2,3]azepino[4,5-b]indole-9-carboxamide (29a)

Yield: 13.5 %; ^{1}H NMR (400 MHz, DMSO-d_6, ppm): δ 11.84 (s, 1H), 10.15 (s, 1H), 8.98 (s, 1H), 8.40–8.31 (m, 2H), 8.26 (m, 1H), 7.83–7.76 (m, 1H), 7.74–7.71 (m, 2H), 7.46–7.33 (m, 6H), 7.31–7.25 (m, 2H), 5.13–5.12 (m, 1H), 4.91 (t, J = 7.2 Hz, 1H), 4.52 (d, J = 9.6 Hz, 1H), 4.42 (t, J = 8.0 Hz,1H), 4.27 (bs, 1H), 3.60–3.53 (m, 5H), 3.30–3.27 (m, 2H), 2.43 (s, 3H), 2.26–2.24 (m, 1H) 2.15–2.08 (m, 1H), 2.00–1.90 (m,

1H), 1.80–1.78 (m, 1H), 1.54–147 (m, 4H), 1.37–1.23 (m, 6H), 0.93 (s, 9H); ^{13}C NMR (400 MHz, DMSO-d_6, ppm); δ 172.15, 171.58, 170.68, 169.64, 166.81, 151.55, 144.71, 138.82, 135.567, 133.69, 131.15, 129.70, 128.85, 128.35, 126.93, 126.40, 125.97, 125.85, 123.80, 122.56, 122.39, 121.91, 117.47, 110.97, 108.43, 68.79, 58.570, 56.38, 47.73, 40.12, 39.07, 38.86, 35.20, 34.910, 31.68, 29.30, 28.53, 26.47, 25.48, 22.50, 16.01; LCMS: m/z = 846.50 [M+H]$^+$; HR-ESIMS; m/z, 846.8234 calcd for $C_{47}H_{55}N_7O_6S+H^+$ (846.0600); HPLC purity 95.29 %.

3.1.12. N-(11-(((S)-1-((2R,4R)-4-hydroxy-2-(((S)-1-(4-(4-methylthiazol-5-yl)phenyl)ethyl) carbamoyl)pyrrolidin-1-yl)-3,3-dimethyl-1-oxobutan-2-yl)amino)-11-oxoundecyl)-6-oxo-5,6,7,12-tetrahydrobenzo[2,3]azepino[4,5-b] indole-9-carboxamide (29b)

Yield: 23.7 %; ^{1}H NMR (400 MHz, DMSO-d_6, ppm); δ 11.82 (s, 1H), 10.14 (s, 1H), 8.97 (s, 1H), 8.38–8.35 (m, 2H), 8.26 (bs, 1H), 7.80–7.71 (m, 3H), 7.45–7.34 (m, 6H), 7.32–7.25 (m, 2H), 5.09 (d, J = 3.6 Hz, 1H), 4.94–4.89 (m, 1H), 4.51 (d, J = 9.2 Hz, 1H), 4.40 (t, J = 4.0 Hz, 1H), 4.27 (bs, 1H), 3.59–3.40 (m, 4H), 3.29–3.25 (m, 2H), 2.45 (s, 3H), 2.32–2.22 (m, 1H), 2.11–2.09 (m, 1H), 2.00–1.99 (m, 1H), 1.80–1.77 (m, 1H), 1.55–1.53 (m, 2H),1.48–1.45 (m, 2H), 1.37–1.25 (m, 15H), 0.92 (s, 9H);^{13}C NMR (400 MHz, DMSO-d_6, ppm): δ 173.88, 172.73, 171.57, 170.88, 170.50, 168.31, 164.81, 156.15, 152.50, 148.83, 145.16, 141.21, 141.02, 135.79, 129.54, 127.08,123.18, 118.16, 111.94, 109.09, 69.50, 67.69, 59.33, 57.40, 54.19, 48.59, 38.86, 35.80, 29.46, 29.35, 26.92, 17.21, 16.39; LCMS: m/z = 902.30 [M+H]$^+$; HR-ESIMS; m/z, 902.6116 calcd for $C_{51}H_{63}N_7O_6S+H^+$ (902.1860); HPLC purity 99.12 %.

3.1.13. N-(12-(((S)-1-((2R,4R)-4-hydroxy-2-(((S)-1-(4-(4-methylthiazol-5-yl)phenyl)ethyl)carbamoyl)pyrrolidin-1-yl)-3,3-dimethyl-1-oxobutan-2-yl)amino)-12-oxododecyl)-6-oxo-5,6,7,12-tetrahydrobenzo[2,3]azepino[4,5-b]indole-9-carboxamide (29c)

Yield: 14.81 %; ^{1}H NMR (400 MHz, DMSO-d_6); δ ppm 11.84 (s, 1H), 10.16 (s, 1H), 8.98 (s, 1H), 8.40–8.36 (m, 2H), 8.26 (bs, 1H), 7.81–7.71 (m, 3H),7.45–7.43 (m, 3H), 7.42–7.34 (m, 3H), 7.31–7.25 (m, 2H), 5.11 (d, J = 3.2 Hz, 1H), 4.91 (t, J = 7.2 Hz, 1H), 4.51 (d, J = 9.6 Hz, 1H), 4.41 (t, J = 8.0 Hz, 1H), 4.26 (bs, 1H), 3.63–3.55 (m, 4H), 3.30–3.25 (m, 2H), 2.45 (s, 3H), 2.33–2.22 (m, 1H), 2.10–1.93 (m, 2H), 1.79–1.76 (m, 1H), 1.56–1.53 (m, 4H), 1.37–1.23 (m, 17H). 0.92 (bs, 9H); ^{13}C NMR (400 MHz, DMSO-d_6, ppm): δ 172.65, 171.89, 170.93, 169.88, 167.23, 151.80, 151.69, 144.68, 129.06, 127.09, 126.60, 124.16, 122.62, 117.66, 111.26, 108.63, 68.98, 68.55, 58.79, 56.67, 56.48, 47.99, 47.69, 40.12, 38.86, 37.88, 35.39, 35.12, 34.78, 34.153, 31.77, 29.17, 29.05, 28.82, 26.76, 26.67, 26.61, 25.65, 22.60, 22.46, 16.14; LCMS: m/z = 916.85 [M+H]$^+$; HR-ESIMS: m/z, 916.6864 calcd for $C_{52}H_{65}N_7O_6S+H^+$ (916.1950); HPLC purity 96.34 %.

3.2. Biological screening

3.2.1. Cell proliferation assay using MCF-7 and A549 cells

MCF-7 and A549 cells were used for the cell proliferation assay. Eagle's Minimum Essential Medium (EMEM) supplemented with (10 %) FBS, (1 %) Pen-Strep, recombinant insulin (0.01 mg/ml) and F12K-ATCC supplemented with (10 %) FBS, and (1 %) Pen-Strep were used as media for MCF-7 and A549 cells, respectively [58]. On day 0, 500 cells per well were seeded in 384-well white plates. On day 1, the cells were treated with PROTAC compounds at varying concentrations (10 fold, 4 points). Different concentrations of compounds were added to the assay plate. The plate was incubated for 72 h at 37 °C, and 5 % CO_2. On day 3, 40 μL of CellTiter Glo-Promega was added to the wells in the assay plate. An EnVision plate reader (Luminescence 700 nm) was used to obtain the read, and the data was analyzed using Xcelfitsoft (REF). Cytotoxicity was analyzed with reference to DMSO control.

3.3. Western blot technique

3.3.1. Seeding, cell lysis and protein extraction

Western blotting with MCF-7cells: A total of 1.5 million cells were seeded in a 6 well plate and incubated overnight at 37 °C with 5 % CO_2. This incubation allowed the cells to adhere and maintain their morphology. The next day, the cells were treated with PROTAC **23a**, at concentrations of range 0.1 to 100 μM. After treatment, the cells were incubated for 16 h and harvested at 1200 rpm for 5 min. The cell pellet was washed twice with PBS and 50 μL of lysis buffer was added to the pellet, which was kept on ice for 30 min with intermittent vortexing. The cell lysate was spun at 13,000 rpm for 15 min for the protein extraction. The protein estimation was performed using a Pierce BCA kit.

3.3.2. Protocol of western blotting

Protein (30 μg) or sample was loaded onto a 4–12 % gradient gel along with a Page Ruler™ Pre-stained Protein Ladder (10 to 180 kDa). The gel was run at 120 V for 2.5 hand protein was transferred into a Polyvinylidene fluoride (PVDF) membrane using an iBlot transfer device. The PVDF membrane was blocked with 5 % skim milk in TBST for 1 h. The membrane was washed three times with TBST. The wash buffer was removed, and primary antibodies against both Vinculin (Rabbit-Mab) and anti-CDK1 antibody, Rabbit Polyclonal (1:1000) in 5 % BSA were added. The membrane was incubated overnight at 4 °C. After overnight incubation the membrane was washed three times with TBST (1 wash - 10 min). The secondary peroxidase AffiniPure goat anti-rabbit IgG (H + L) (1:10,000) in 5 % BSA was added to the membrane and the membrane was incubated for 1 h at RT. The membrane was washed three times with TBST and the blots were developed using Chemi Doc software with Pierce ECL Western Blotting Substrate.

3.4. Molecular modelling study

To identify the suitable binding site for tethering in the CDK1 inhibitor, a molecular docking study was carried out to mimic the interaction of newly designed paullone based PROTAC ligands and paullone with the CDK1 protein at the atomic level.

3.4.1. Ligand preparation

The ligands were prepared using LigPrep (Schrodinger, LLC, NY, USA), where all possible states at a target pH 7.0 –2.0 with partial atomic charges were generated [59,60]. The geometry of the ligands was then optimized by energy minimization using the Optimum Potentials for Liquid Simulation 4 (OPLS4) force field, until a gradient of 0.01 kcal /mol/Å was reached.

3.4.2. Protein preparation

The three-dimensional structure of CDK1 (PDB: 6GU6) was retrieved from the RCSB protein data bank (https://www.rcsb.org). The protein was prepared using the protein preparation wizard in Maestro (GUI for Schrödinger) which removes the hydrogen atoms, and water molecules from the 3D crystal structure of the protein [61]. Furthermore, the protein energy was minimized using the OPLS4 force field until the root mean square deviation (RMSD) converged to 0.1 Å.

3.4.3. Grid generation and validation

The receptor grid of the prepared CDK1 target was generated using the Schrödinger suite's grid generation module. The size of the inner grid box was defined as 10 Å × 10 Å × 10 Å and the size of the outer grid box was defined as 20 × 20 × 20 Å from the centroid of the co-crystallized ligand [62–65]. The docking protocol was validated by redocking the native ligand of the target protein. Molecular docking was carried out using the Schrödinger suite GLIDE (Grid-based Ligand Docking with Energetics). The molecules were subjected to extra precision (XP) docking keeping all the values at their defaults. Maestro structure analysis was used to visualize and analyze the results. The
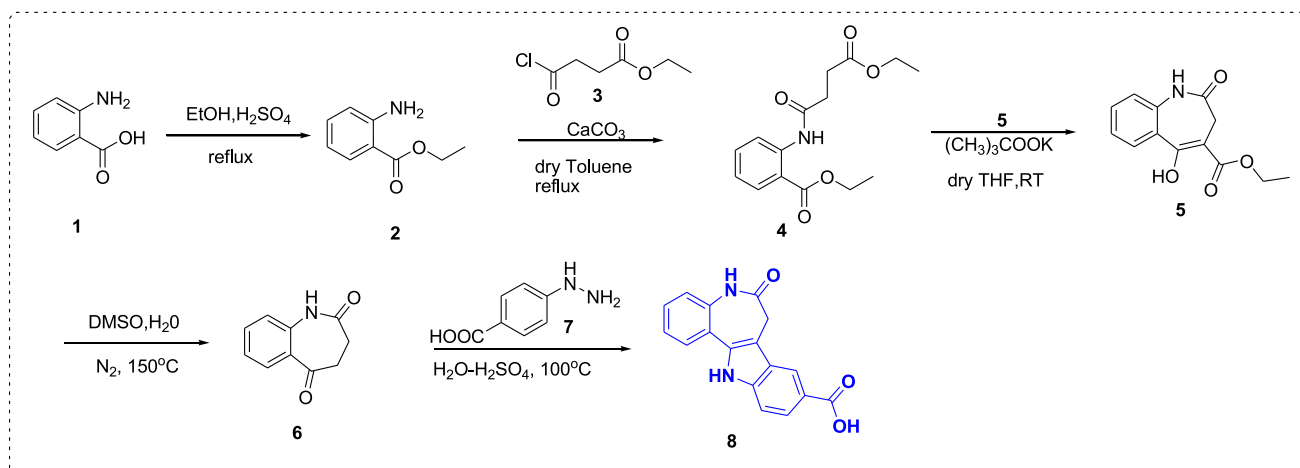
Scheme 1. Synthesis of paullone carboxylic acid.
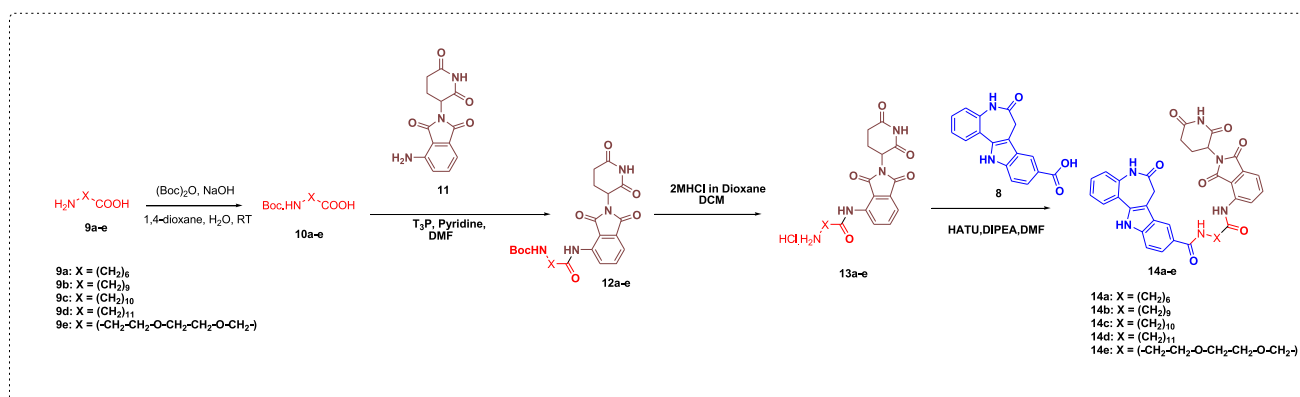
Scheme 2. Synthesis of PROTACs **14a-e**.

Discovery Studio Visualizer 2021 was utilized for receptor surface analysis.

3.5. Binding free energy estimation using the molecular mechanics-generalized born surface area (MM-GBSA) approach

The free energy of the binding of paullone and the most active paullone based PROTAC ligand PROTAC **23a** to the CDK1 protein was calculated using the MM-GBSA protocol [66]. In this case, molecular mechanics are utilized in combination with Generalized Born and Surface Continuum implicit solvent models to estimate the binding free energy. The Prime/MM-GBSA algorithm incorporates OPLS4 force field, VSGB solvent model[3], and rotamer search. The Prime/MM-GBSA (ΔG) was estimated by keeping all the protein atoms rigid, and setting the
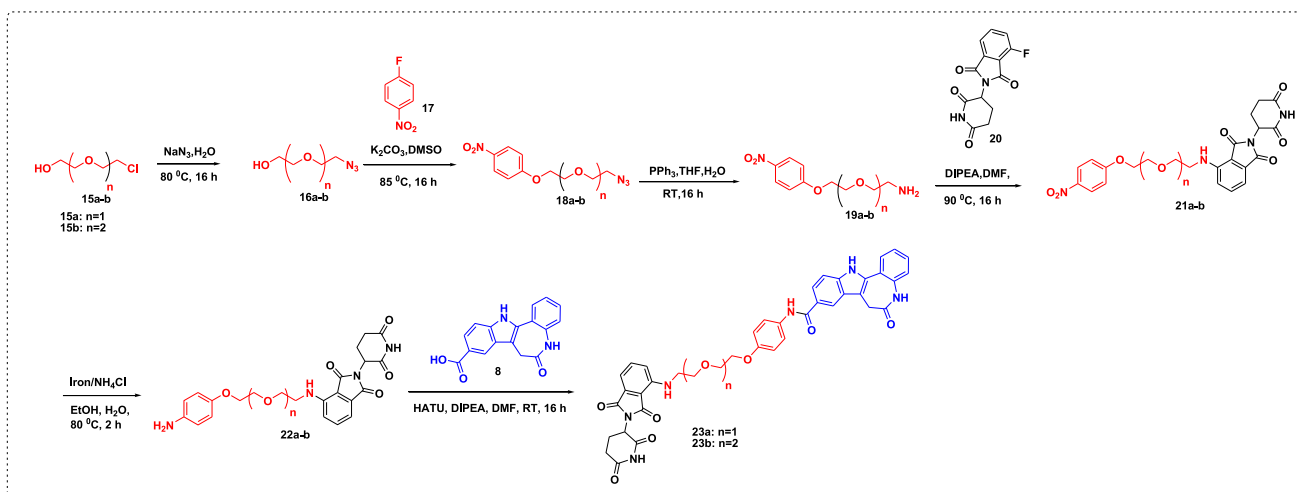
Scheme 3. Synthesis of desired PROTACs **23a-b**.
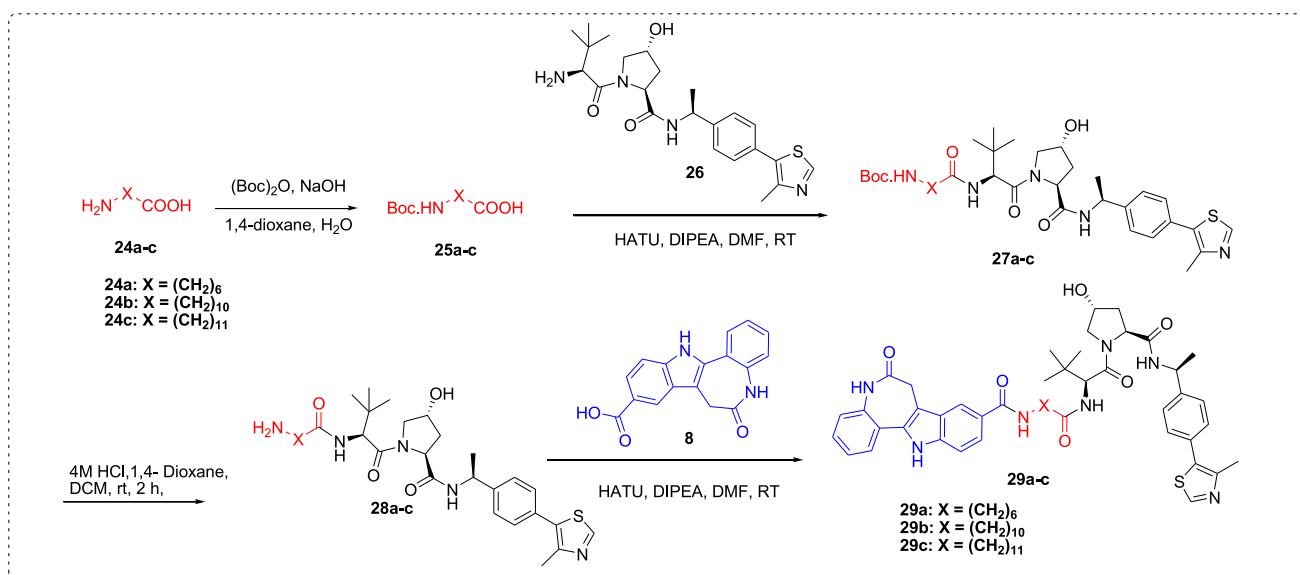
Scheme 4. Synthesis of desired PROTACs **29a-c.**

ligand atoms flexible, based on the following relationship.

$$\Delta G_{binding} = E_{complex(Minimized)} - E_{ligand(Minimized)} - E_{protein(Minimized)}$$

where, "$E_{complex}$" is the total free energy of the protein-ligand complex and "$E_{protein}$" and "E_{ligand}" are the free energies of the protein and ligand in the solvent, respectively. The free energies of binding obtained from the MM/GBSA protocol are approximate energies; a more negative value indicates stronger ligand receptor binding.

4. Results and discussion

4.1. Chemistry

To test the feasibility of our hypothesis, paullone carboxylic acid 8 was chosen as a key intermediate for designing PROTACs (Scheme 1). Initially, 3,4-dihydro-1*H*-benzo[*b*]azepine-2,5-dione 6 was prepared by using a previously reported method [42]. Fischer indole synthesis was then employed to introduce a carboxylic group on the paullones through reaction with 4-hydrazinobenzoic acid 7 [67]. The reaction was then optimized using solvents of different polarities. We used aqueous sulfuric acid at 100 °C to obtain the desired paullone carboxylic acid 8 in 76 % yield.

With key intermediate paullone carboxylic acid **8**, the first batch of PROTACs was designed by attaching compound **8** to thalidomide through linear linkers of various lengths (Scheme 2). First, amino substituted thalidomide **11** was coupled with Boc-protected carboxylic acids **10a-e** to give amides **12a-e**. The deprotection of the Boc group of compounds **12a-e** under acidic conditions provided amine hydrochloride salts **13a-e**. Finally, the coupling of paullone carboxylic acid **8** and amine hydrochloride **13a-e** using the HATU coupling reagent provided the desired PROTACs **14a-e.**

We next introduced the aromatic substituted polyethylene glycol linkers **18a-b** in two steps (Scheme 3). Azidation of 2-chloropolyethoxyethanols **15a-b** afforded **16a-b**, which were then coupled with 4-flouronitrobenzene **17** to give **18a-b**. The reduction of azides **18a-b**, in the presence of triphenylphosphine, leads to the formation of amine intermediates **19a-b**, which are subsequently coupled with fluoro substituted thalidomide **20** to obtain **21a-b**. The reduction of the nitro group of **21a-b** with Fe/NH$_4$Cl provided amines **22a-b**. Finally, the desired PROTACs **23a-b** are synthesized by coupling amines **22a-b** with the key intermediate paullone carboxylic acid **8**.

Although most clinical drugs are reported with CRBN ligands, VHL

Table 1
In-vitro activity results of selected PROTACs against MCF-7 and A549 cells.

S. no.	Compound	MCF-7 IC$_{50}$ (μM)	A549 IC$_{50}$ (μM)
1	**8**	*	4.0
2	**23a**	0.10	0.12
3	**14c**	5.3	*
4	**14d**	6.6	*
5	Doxorubicin	0.73	3.64

* IC$_{50}$ values could not be calculated because of maximum cytotoxicity was below 70 % at 10 μM.

ligands have their advantages. VHL E3 ligase has different expression levels in different cells and is more stable. Thus, we next investigated the synthetic route for VHL-based paullone PROTACS **29a-c** as illustrated in Scheme 4. The Boc protection of amino acids **24a-c** produced compounds **25a-c**, which were coupled with VHL ligand **26** to yield compounds **27a-c**. Then deprotection of the Boc group under acidic conditions produced amines **28a-c**. Finally, amines **28a-c** reacted with intermediate **8** to generate the final PROTACs **29a-c.**

4.2. Antiproliferative activity

We investigated the cytotoxicity of the synthesized PROTACs in both MCF-7 (human breast cancer) and A549 (human lung cancer) cells [68]. As cell permeability is more crucial for PROTAC compounds with higher molecular weights than conventional small-molecule inhibitors, we screened the synthesized compounds through the MTT assay. Cell growth inhibition was measured using different concentrations of the PROTAC compounds, and the measured absorbance values were normalized to those of DMSO-treated cells. The IC$_{50}$ values were further determined through growth inhibition curves generated with various concentrations of selected PROTAC compounds.

Breast cancer cells (MCF-7) were treated with four different concentrations (0.1–100 μM, 4 points) of synthesized PROTACs. The detailed results of the four-point inhibition of MCF-7 cells by synthesized PROTAC compounds are included in the supporting information Table S1. A series of synthesized PROTAC compounds **23a, 14d** and **14c** showed >50 % inhibition at a lower concentration in a four-point inhibition assay against MCF-7 cells. The three PROTACs with significant inhibitory potential in the initial screening were further tested at ten different concentrations ranging from 0.0015 to 30 μM for 72 h in a cell
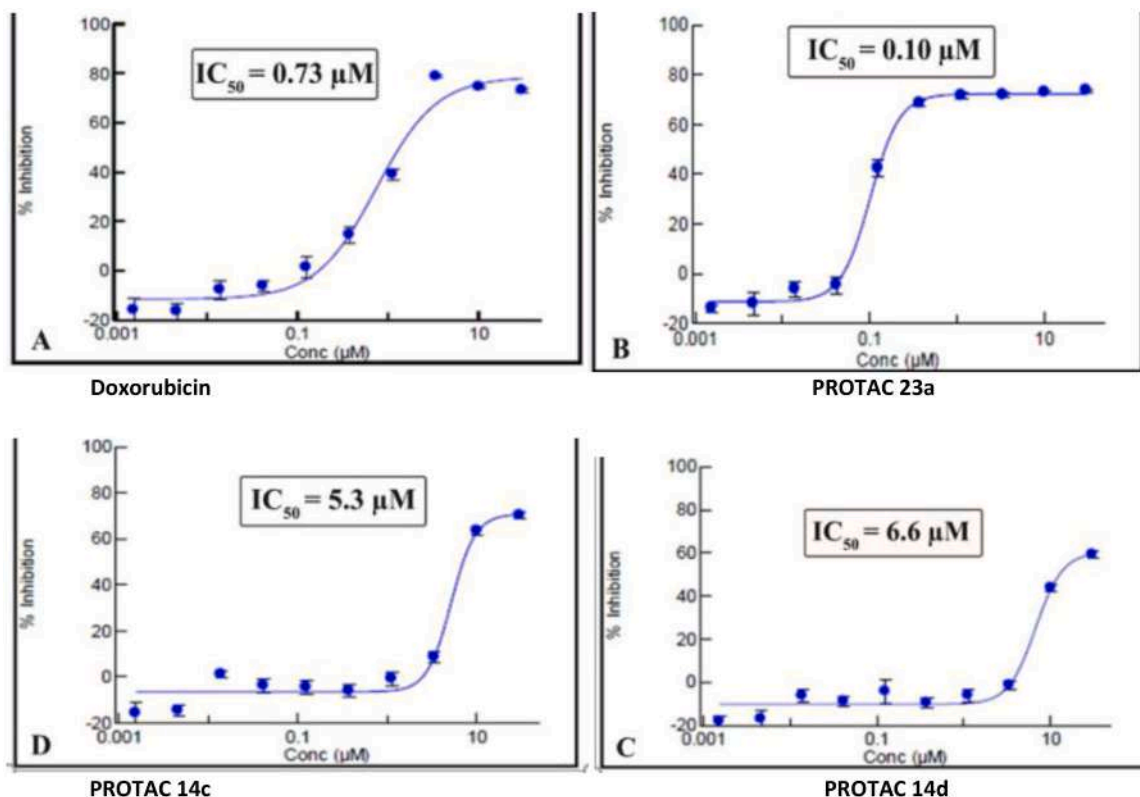
Fig. 2. In-vitro antiproliferative activity of synthesized PROTACs and the standard drug (doxorubicin) in MCF-7 cells.

proliferation assay. These selected analogues significantly inhibited MCF-7 cells with IC$_{50}$ values (**23a**, IC$_{50}$ = 0.10 μM; **14d**, IC$_{50}$ = 6.6 μM; **14c**, IC$_{50}$ = 5.3 μM) (Table 1). In-vitro assay results proved that these PROTAC compounds are more effective against breast cancer than the standard drug doxorubicin (Fig. 2). Importantly, the paullone based PROTAC **23a** displayed significantly improved antiproliferative activity compared to that of paullone carboxylic acid **8**, suggesting the potential advantage of the PROTAC as a CDK1 degrader for breast cancer therapy.

To understand the efficacy of PROTACs against lung cancer, the compounds are tested against human lung cancer A549 cells at four different concentrations ranging from 0.1 to 100 μM. Among all the synthesized compounds, PROTAC **23a** showed significant growth inhibition with IC$_{50}$ = 0.12 μM (Table 1). Furthermore, paullone carboxcylic acid **8** exhibited less activity with IC$_{50}$ = 4 μM compared to PROTAC **23a**. These results indicated the importance of PROTAC for the antiproliferative activity. The composition of linkers affects antiproliferative activity. PROTACs with linear aliphatic and PEG linkers showed no significant activity. Whereas rigidifying the linker with phenyl substituted polyethylene glycol chains in PROTAC **23a** resulted in

increased activity. PROTAC **23a** disclosed in this study represents the potent anti-cancer agent, which could serve as a valuable chemical probe for further evaluation of its therapeutic potential in breast and lung cancer therapy.

4.3. Western blotting

Western blotting analysis was then used to investigate the degradation of the CDK1 protein by PROTAC **23a**. MCF-7 cells were treated with **23a**, at concentrations ranging from 0.003 to 50 μM, and cells were incubated for 16 h before harvesting [69]. Housekeeping gene expression was consistent across all the concentrations tested. Target protein levels were detected by western blot analysis. Protein levels were normalized to those of a housekeeping gene (Vinculin) and DMSO controls. Across all tested concentrations Vinculin did not show any modulation. PROTAC **23a** showed a concentration dependent degradation of CDK1 from 5.5 to 16 μM. As observed in multiple PROTACs in literature PROTAC **23a** also showed hook effect at 50 μM (Fig. 3). In the case of PROTAC **23a**, rigidifying the linker through phenyl substituted
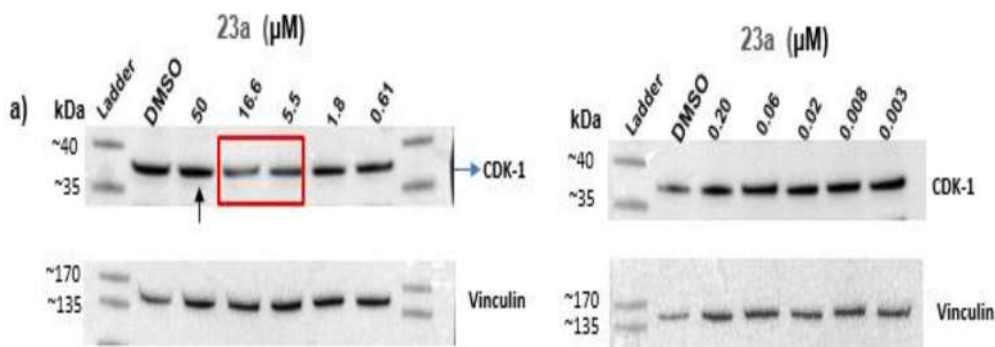
Fig. 3. Western blot (CDK1 and Vinculin) after 16 h of treatment with the PROTAC **23a**.
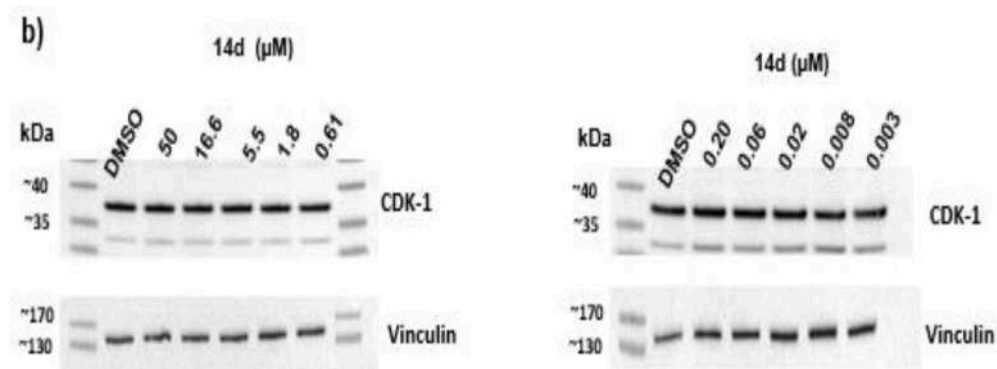
Fig. 4. Western Blot (CDK1 and Vinculin) after 16 h treatment with **14d**.
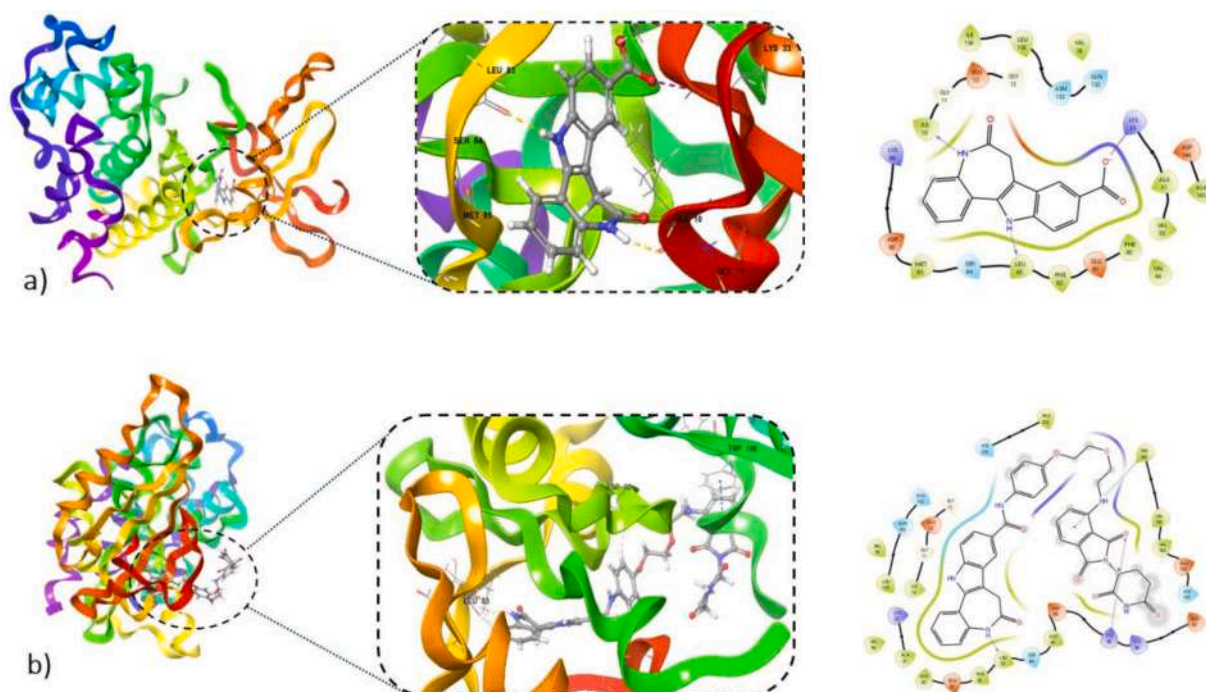
Fig. 5. 2D and 3D binding interaction images of A) Paullone carboxylic acid 8 and B) Paullone PROTAC **23a** in the active site of the CDK1 enzyme (PDB: 6GU6).

PEG chain may led to a stable ternary complex formation and potent CDK1 protein degradation.

Another PROTAC compound **14d** was also evaluated for its ability to degrade the CDK1 protein in MCF-7 cells. PROTAC **14d** caused a marginal decrease in CDK1 expression at different concentrations tested (Fig. 4). Weaker cytotoxic activity of PROTAC **14d** can be corroborated with its weak CDK1 degradation potential.

4.4. Molecular docking

A docking study was performed to gain insight into the ligand-receptor interactions of paullone carboxylic acid **8** and most active paullone based PROTAC **23a** ligands with CDK1 [70,71]. The docking protocol was tested and verified by re-docking the co-crystallized native ligand in the binding pocket, which showed a binding affinity of −10.27 kcal/mol with an RMSD-1.32 Å. The 3D and 2D ligand interactions of paullone carboxylic acid **8** and the most active PROTAC **23a** with CDK1 are depicted in Fig. 5. Paullone carboxylic acid **8** and PROTAC **23a** showed binding affinities with dock scores of −9.13 kcal/mol and −5.76 kcal/mol respectively. A detailed analysis of the hydrogen bonding and hydrophobic interactions between paullone and the binding site of

CDK1 revealed the following interactions (Fig. 5A); the side chain of LYS-33 forms H-bond electrostatic interactions with the carboxylate group of paullone (2.46 Å and 2.28 Å). LEU-83 forms a hydrogen bond with the NH of the indole ring (1.89 Å), ILE-10 forms a hydrogen bond with the NH of the azepinone ring of paullone (1.73 Å). PHE-82 shows hydrophobic interactions through π-π stacking (5.72 Å) and ASP-86 makes the pi-anion electrostatic interaction with the phenyl ring of the ligand. However, LEU-135, ALA-31 and ILE-10 exhibited hydrophobic interactions through π-alkyl interactions with ligand. In addition, the SER-89, SER-84, VAL-18, VAL-64 and PHE-80 residues participate van der Waals interactions with the phenyl ring of the ligand. Likewise, PROTAC **23a** showed the following hydrogen bonding and hydrophobic interactions with the binding site of CDK1 (Fig. 5B); the side chain of LEU-83 forms an H-bond with the NH of azepinone ring of paullone (2.21 Å) and LYS-88 forms an H-bond with isoindole (2.21 Å). Residue PHE-82 showed hydrophobic interactions through π-π stacking interactions (5.87 Å) with the phenyl ring of paullone. In addition to these residues ALA-31, ILE-10 and LEU-135 exhibit π-alkyl hydrophobic interactions. Residues PHE-80, VAL-18, VAL-64 and MET-85 participate in van der Waals interactions with the phenyl ring of the paullone ligand. Furthermore, it has been observed that the thalidomide (E3 ligase
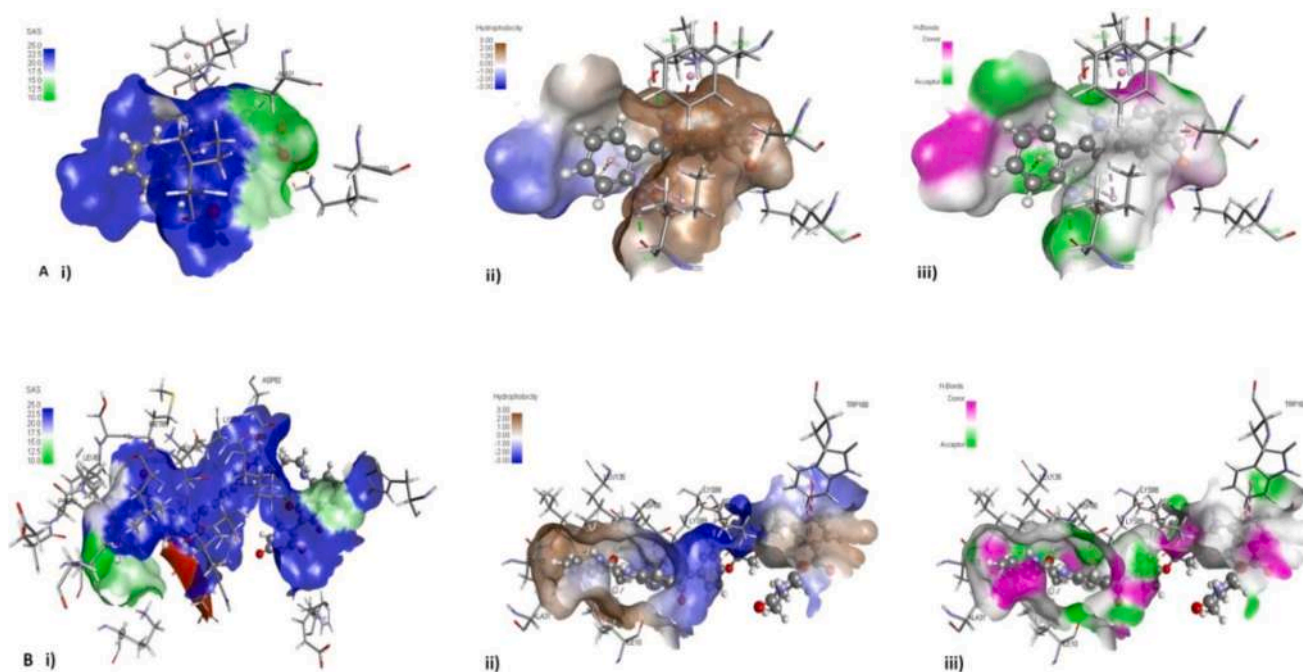
Fig. 6. (i) Solvent accessibility surface (SAS) (ii) Hydrophobic surface; and (iii) Hydrogen bond donor/acceptor of the CDK1 receptor with A) Paullone carboxylic acid 8 and B) PROTAC **23a**.

Table 2
MM-GBSA analysis for binding free energy calculations.

Compounds	MM-GBSA (kcal/mol)			
	Cyclic Dependent Kinase 1 enzyme (PDB: 6GU6)			
	ΔG_{bind}	$\Delta G_{bind\ coulomb}$	$\Delta G_{bind\ lipo}$	$\Delta G_{bind\ vdW}$
Native ligand	−63.10	−16.85	−19.13	−54.16
8	−20.84	−02.42	−12.11	−43.45
23a	−49.06	−14.67	−16.84	−61.60

ΔG_{bind}, binding free energy; $\Delta G_{bind\ coulomb}$, Coulombic interaction energy; $\Delta G_{bind\ lipo}$, lipophilic interaction energy; $\Delta G_{bind\ vdW}$, Van der Waals interaction energy.

ligand) substituted on the indole ring of paullone through linker extends the designed PROTAC into the solvent accessible region, increasing its potential to interact with the E3 ligase as depicted in Fig. 5B. The hydrogen bond donor/acceptor, hydrophobic and solvent accessibility surface (SAS) surfaces were generated within 5 Å of the paullone carboxylic acid **8** and PROTAC **23a** atoms to obtain unique insight into the inner workings of CDK1 and are depicted in Fig. 6A and B.

4.5. Binding free energy estimation using MM GBSA approach

The binding free energy of the CDK1 paullone carboxylic acid **8** and paullone PROTAC **23a** docked complex was estimated by determining the molecular mechanics general born surface area (MM-GBSA) [72]. The ΔG_{bind} values of the native ligand, **8** and PROTAC **23a** are shown in Table 2. The MM-GBSA ΔG_{bind} values of the paullone carboxylic acid **8** and PROTAC **23a** molecules were found to be −20.84 kcal/mol and −49.06 kcal/mol respectively. However, the binding free energy of the native ligand is −63.10 kcal/mol. These results suggest that PROTAC **23a** forms a more stable complex with CDK1 than does Paullone carboxylic acid **8**.

5. Conclusion

PROTACs are a promising treatment option for cancer that has drawn a lot of interest. We combined synthetic, computational and in-vitro protocols to develop novel paullone based PROTACs. We synthesized different substituted paullone-based PROTACs and characterized them using multiple spectroscopic techniques. These PROTACs were then screened against both the MCF-7 and A549 cell lines. In the initial screening, we observed that these PROTACs are more effective against the MCF-7 and A549 cell lines. Among the synthesized, PROTAC **23a** and **14d** have shown potent antiproliferative activity and thus, were subjected to western blot analysis to measure CDK1 degradation. Western blotting confirmed that these compounds are CDK1 degraders and antiproliferative effects are achieved through downregulating the CDK1 protein. Molecular docking of PROTACs at CDK1 also confirmed that these compounds have excellent binding affinity for the CDK1 protein to initiate antiproliferative effects. Our findings suggested that PROTAC **23a** is an effective paullone-based CDK1 degrader with potential for treating breast and lung cancer. In addition, the PROTAC approach utilized in this study will pave the way for the structural optimization of more paullone-based PROTACs as anticancer agents. Further studies to extend the application of this paullone-based PROTAC library toward PROTAC drugs are in progress in our laboratory.

Declaration of competing interest

The authors declare that they have no conflict of interest.

Supplementary materials

Supplementary material associated with this article can be found, in the online version, at doi:10.1016/j.molstruc.2024.141273.

Data availability

Data will be made available on request.

References

[1] C.N. Sternberg, K. Fizazi, F. Saad, N.D. Shore, U. De Giorgi, D.F. Penson, U. Ferreira, E. Efstathiou, K. Madziarska, M.P. Kolinsky, D.I.G. Cubero, B. Noerby, F. Zohren, X. Lin, K. Modelska, J. Sugg, J. Steinberg, M. Hussain, Enzalutamide and survival in nonmetastatic, castration-resistant prostate cancer, N. Engl. J. Med. 382 (2020) 2197–2206, https://doi.org/10.1056/NEJMoa2003892.

[2] P.A. Watson, V.K. Arora, C.L. Sawyers, Emerging mechanisms of resistance to androgen receptor inhibitors in prostate cancer, Nat. Rev. Cancer 15 (2015) 701–711, https://doi.org/10.1038/nrc4016.

[3] J. Schmitt, S. Huang, E. Goodfellow, C. Williams, B.J. Jean-Claude, Design and synthesis of a trifunctional molecular system "programmed" to block epidermal growth factor receptor tyrosine kinase, induce high levels of DNA damage, and inhibit the DNA repair enzyme (poly(ADP-ribose) polymerase) in prostate cancer cells, J. Med. Chem. 63 (2020) 5752–5762, https://doi.org/10.1021/acs.jmedchem.9b02008.

[4] T. Di Desidero, A. Fioravanti, P. Orlandi, B. Canu, R. Giannini, N. Borrelli, S. Man, P. Xu, G. Fontanini, F. Basolo, R.S. Kerbel, G. Francia, R. Danesi, G. Bocci, Antiproliferative and proapoptotic activity of sunitinib on endothelial and anaplastic thyroid cancer cells via inhibition of Akt and ERK1/2 phosphorylation and by down-regulation of cyclin-D1, J. Clin. Endocrinol. Metab. 98 (2013) E1465–E1473, https://doi.org/10.1210/jc.2013-1364.

[5] J. Zhu, X. Jiang, X. Luo, R. Zhao, J. Li, H. Cai, X.Y. Ye, R. Bai, T. Xie, Combination of chemotherapy and gaseous signaling molecular therapy: novel β-elemene nitric oxide donor derivatives against leukemia, Drug Dev. Res. 84 (2023) 718–735, https://doi.org/10.1002/ddr.22051.

[6] J. Dai, J. Gao, H. Dong, Prognostic relevance and validation of ARPC1A in the progression of low-grade glioma, Aging (Albany NY) 16 (2024) 11162–11184, https://doi.org/10.18632/aging.205952.

[7] L. Zhang, H. Shi, X. Tan, Z. Jiang, P. Wang, J. Qin, Ten-gram-scale mechanochemical synthesis of ternary lanthanum coordination polymers for antibacterial and antitumor activites, Front. Chem. 10 (2022) 898324, https://doi.org/10.3389/fchem.2022.898324.

[8] W. Wang, C. Liu, J. Luo, L. Lei, M. Chen, Y. Zhang, R. Sheng, Y. Li, L. Wang, X. Jiang, T. Xiao, Y. Zhang, S. Li, Y. Wu, Y. Xu, Y. Xu, A novel small-molecule PCSK9 inhibitor E28362 ameliorates hyperlipidemia and atherosclerosis, Acta Pharmacol. Sin. 45 (2024) 2119–2133, https://doi.org/10.1038/s41401-024-01305-9.

[9] C.H. Jiang, T.L. Sun, D.X. Xiang, S.S. Wei, W.Q. Li, Anticancer activity and mechanism of xanthohumol: a prenylated flavonoid from Hops (*Humulus lupulus* L.), Front. Pharmacol. 9 (2018) 530, https://doi.org/10.3389/fphar.2018.00530.

[10] Y. Nie, D. Li, Y. Peng, S. Wang, S. Hu, M. Liu, J. Ding, W. Zhou, Metal organic framework coated MnO$_2$ nanosheets delivering doxorubicin and self-activated DNAzyme for chemo-gene combinatorial treatment of cancer, Int. J. Pharm. 585 (2020) 119513, https://doi.org/10.1016/j.ijpharm.2020.119513.

[11] L. Kang, X.H. Gao, H.R. Liu, X. Men, H.N. Wu, P.W. Cui, E. Oldfield, J.Y. Yan, Structure-activity relationship investigation of coumarin-chalcone hybrids with diverse side-chains as acetylcholinesterase and butyrylcholinesterase inhibitors, Mol. Divers. 22 (2018) 893–906, https://doi.org/10.1007/s11030-018-9839-y.

[12] X.H. Gao, J.J. Tang, H.R. Liu, L.B. Liu, Y.Z. Liu, Structure-activity study of fluorine or chlorine-substituted cinnamic acid derivatives with tertiary amine side chain in acetylcholinesterase and butyrylcholinesterase inhibition, Drug Dev. Res. 80 (2019) 438–445, https://doi.org/10.1002/ddr.21515.

[13] Q. Lu, Y. Chen, H. Liu, J. Yan, P. Cui, Q. Zhang, X. Gao, X. Feng, Y. Liu, Nitrogen-containing flavonoid and their analogs with diverse B-ring in acetylcholinesterase and butyrylcholinesterase inhibition, Drug Dev. Res. 81 (2020) 1037–1047, https://doi.org/10.1002/ddr.21726.

[14] K. Wang, J. Yin, J. Chen, J. Ma, H. Si, D. Xia, Inhibition of inflammation by berberine: molecular mechanism and network pharmacology analysis, Phytomedicine 128 (2024) 155258, https://doi.org/10.1016/j.phymed.2023.155258.

[15] M. Hashemi, M. Razzazan, M. Bagheri, S. Asadi, B. Jamali, M. Khalafi, A. Azimi, S. Rad, M. Behroozaghdam, N. Nabavi, M. Rashidi, F. Dehkhoda, A. Taheriazam, M. Entezari, Versatile function of AMPK signaling in osteosarcoma: an old player with new emerging carcinogenic functions, Pathol. - Res. Pract. 251 (2023) 154849, https://doi.org/10.1016/j.prp.2023.154849.

[16] P. Nurse, Y. Masui, L. Hartwell, Understanding the cell cycle, Nat. Med. 4 (1998) 1103–1106, https://doi.org/10.1038/2594.

[17] C.J. Sherr, Cancer cell cycles, Science 274 (1996) 1672–1677, https://doi.org/10.1126/science.274.5293.167.

[18] S. Lim, P. Kaldis, Cdks, cyclins and CKIs: roles beyond cell cycle regulation, Development, 140 (2013) 3079–3093, https://doi.org/10.1242/dev.091744.

[19] T. Hunt, K. Nasmyth, B. Novak, Introduction: the cell cycle, Philos. Trans. R. Soc. B 366 (2011) 3494–3497, https://doi.org/10.1098/rstb.2011.027.

[20] T. Hunt, Synthesis, proteolysis, and cell cycle transitions, Biosci. Rep. 22 (2002) 465–486, https://doi.org/10.1023/A:1022077317801.

[21] E.G. Nabel, CDKS and CKIS: molecular targets for tissue remodelling, Nat. Rev. Drug Discov. 1 (2002) 587–598, https://doi.org/10.1038/nrd869.

[22] E. Sausville, Cyclin-dependent kinase modulators studied at the NCI: pre-clinical and clinical studies, Curr. Med. Chem. Anti-Cancer Agents 3 (2003) 47–56, https://doi.org/10.2174/1568011033353560.

[23] J.K. Buolamwini, Cell cycle molecular targets in novel anticancer drug discovery, Curr. Pharm. Des. 6 (2000) 379–392, https://doi.org/10.2174/1381612003400948.

[24] S. Grant, J. Roberts, The use of cyclin-dependent kinase inhibitors alone or in combination with established cytotoxic drugs in cancer chemotherapy, Drug Resist. Updat. 6 (2003) 15–26, https://doi.org/10.1016/S1368-7646(02)00141-3.

[25] M. Knockaert, P. Greengard, L. Meijer, Pharmacological inhibitors of cyclin-dependent kinases, Trends Pharmacol. Sci. 23 (2002) 417–425, https://doi.org/10.1016/S01655-6147(02)02071-0.

[26] L. Fischer, J. Endicott, L. Meijer, Cyclin-dependent kinase inhibitors, Prog. Cell Cycle Res. 5 (2003) 235–248.

[27] A. Huwe, R. Mazitschek, A. Giannis, Small molecules as inhibitors of cyclin-dependent kinases, Angew. Chem. Int. Ed. Engl. 42 (2003) 2122–2138, https://doi.org/10.1002/anie.200200540.

[28] P.M. Fischer, A. Gianella-Borradori, CDK inhibitors in clinical development for the treatment of cancer, Expert Opin. Investig. Drugs 12 (2003) 955–970, https://doi.org/10.1517/13543784.12.6.955.

[29] V.A. Smits, R.H. Medema, Checking out the G$_2$/M transition, Biochim. Biophys. Acta 1519 (2001) 1–12, https://doi.org/10.1016/S0167-4781(01)00204-4.

[30] Q. Wang, A.M. Bode, T. Zhang, Targeting CDK1 in cancer: mechanisms and implications, NPJ Precis. Oncol. 7 (2023) 58, https://doi.org/10.1038/s41698-023-00407-7.

[31] G. Massacci, L. Perfetto, F. Sacco, The cyclin-dependent kinase 1: more than a cell cycle regulator, Br. J. Cancer 129 (2023) 1707–1716, https://doi.org/10.1038/s41416-023-02468-8.

[32] L. Minglei, Z. Ying, L. Bo, Y. Qingqiang, Advancing strategies for proteolysis-targeting chimera design, J. Med. Chem. 66 (2023) 2308–2329, https://doi.org/10.1021/acs.jmedchem.2c01555.

[33] T. Wu, Z. Zhang, G. Gong, Z. Du, Y. Xu, S. Yu, F. Ma, Discovery of novel flavonoid-based CDK9 degraders for prostate cancer treatment via a PROTAC strategy, Eur. J. Med. Chem. 260 (2023) 115774, https://doi.org/10.1016/j.ejmech.2023.115774.

[34] D. Nalawansha, C.M. Crews, PROTACs: an emerging therapeutic modality in precision medicine, Cell Chem. Biol. 27 (2020) 998–1014, https://doi.org/10.1016/j.chembiol.2020.07.020.

[35] V. Kumarasamy, Z. Gao, B. Zhao, B. Jiang, S.M. Rubin, K. Burgess, A.K. Witkiewicz, E.S. Knudsen, PROTAC-mediated CDK degradation differentially impacts cancer cell cycles due to heterogeneity in kinase dependencies, Br. J. Cancer. 129 (2023) 1238–1250, https://doi.org/10.1038/s41416-023-02399-4.

[36] X. Sun, Y. Rao, PROTACs as potential therapeutic agents for cancer drug resistance, Biochemistry 59 (2020) 240–249, https://doi.org/10.1021/acs.biochem.9b00848.

[37] H. Gao, X. Sun, Y. Rao, PROTAC technology: opportunities and challenges, ACS Med. Chem. Lett. 11 (2020) 237–240, https://doi.org/10.1021/acsmedchemlett.9b00597.

[38] S. Zeng, W. Huang, X. Zheng, L. Cheng, Z. Zhang, J. Wang, Z. Shen, Proteolysis targeting chimera (PROTAC) in drug discovery paradigm: recent progress and future challenges, Eur. J. Med. Chem. 210 (2021) 112981, https://doi.org/10.1016/j.ejmech.2020.112981.

[39] K. Garber, The PROTAC gold rush, Nat. Biotechnol. 40 (2022) 12–16, https://doi.org/10.1038/s41587-021-01173-2.

[40] M.C. Aublette, T.A. Harrison, E.J. Thorpe, M.S. Gadd, Selective Wee1 degradation by PROTAC degraders recruiting VHL and CRBN E3 ubiquitin ligases, Bioorg. Med. Chem. Lett. 64 (2022) 128636, https://doi.org/10.1016/j.bmcl.2022.128636.

[41] D.W. Zaharevitz, R. Gussio, M. Leost, A. Senderowicz, T. Lahusen, C. Kunick, L. Meijer, E.A. Sausville, Discovery and initial characterization of the paullones, a novel class of small-molecule inhibitors of cyclin-dependent kinases, Cancer Res. 59 (1999) 2566–2569.

[42] C. Schultz, A. Link, M. Leost, D.W. Zaharevitz, R. Gussio, E.A. Sausville, L. Meijer, C. Kunick, Paullones, a series of cyclin-dependent kinase inhibitors: Synthesis, evaluation of CDK1/cyclin B inhibition, and in vitro antitumor activity, J. Med. Chem. 42 (1999) 2909–2919, https://doi.org/10.1021/jm9900570.

[43] D.R. Stuart, P. Alsabeh, M. Kuhn, K. Fagnou, Rhodium(III)-catalyzed arene and alkene C–H bond functionalization leading to indoles and pyrroles, J. Am. Chem. Soc. 132 (2010) 18326–18339, https://doi.org/10.1021/ja1082624.

[44] M. Tobisu, H. Fujihara, K. Koh, N. Chatani, Synthesis of 2-boryl- and silylindoles by copper-catalyzed borylative and silylative cyclization of 2-alkenylaryl isocyanides, J. Org. Chem. 75 (75) (2010) 4841–4847, https://doi.org/10.1021/jo101024f.

[45] Z. Li, N. Lu, L. Wang, W. Zhang, Synthesis of paullone and kenpaullone derivatives by photocyclization of 2-(2-chloro-1*H*-indol-3-yl)-*N*-arylacetamides, Eur. J. Org. Chem. 2012 (2012) 1019–1024, https://doi.org/10.1002/ejoc.201101508.

[46] E.L. Sang, J.L. Seong, C. Cheol-Hong, Concise total syntheses of paullone and kenpaullone via cyanide-catalyzed intramolecular imino-stetter reaction, Synthesis 49 (2017) 4247–4253, https://doi.org/10.1055/s-0036-1588749.

[47] S. Christiane, L. Andreas, L. Maryse, W.Z. Daniel, G. Rick, A.S. Edward, M. Laurent, K. Conrad, Paullones, a series of cyclin-dependent kinase inhibitors: synthesis, evaluation of CDK1/cyclin B inhibition, and in vitro antitumor activity, J. Med. Chem. 42 (1999) 2909–2919, https://doi.org/10.1021/jm9900570.

[48] T. Opatz, D. Ferenc, Synthesis of the CDK-inhibitor paullone by cyclization of a deprotonated α-aminonitrile, Synthesis 24 (2008) 3941–3944, https://doi.org/10.1055/s-0028-1083250.

[49] M. Leost, C. Schultz, A. Link, Y.Z. Wu, J. Biernat, E.M. Mandelkow, J.A. Bibb, G. L. Snyder, P. Greengard, D.W. Zaharevitz, R. Gussio, A.M. Senderowics, E. A. Sausville, C. Kunick, L. Meijer, Paullones are potent inhibitors of glycogen synthase kinase-3β and cyclin-dependent kinase 5/p25, Eur. J. Biochem. 267 (2000) 5983–5994, https://doi.org/10.1046/j.1432-1327.2000.01673.x.

[50] T. Pies, K.J. Schaper, M. Leost, D.W. Zaharevitz, R. Gussio, L. Meijer, C. Kunick, CDK1-inhibitory activity of paullones depends on electronic properties of 9-substituents, Arch. Pharm. Pharm. Med. Chem. 337 (2004) 486–492, https://doi.org/10.1002/ardp.200300870.

[51] K. Wieking, M. Knockaert, M. Leost, D.W. Zaharevitz, L.M. Meijer, CDK1-inhibitory activity of paullones depends on electronic properties of 9-substituents, Arch. Pharm. Pharm. Med. Chem. 7 (7) (2002) 311–317, https://doi.org/10.1002/ardp.200300870.

[52] Z. Yutian, M. Danhui, W. Yinyin, The PROTAC technology in drug development, Cell Biochem. Funct. 37 (37) (2019) 21–30, https://doi.org/10.1002/cbf.3369.

[53] Y. Liang, K.S. Nandakumar, K. Cheng, Design and pharmaceutical applications of proteolysis-targeting chimeric molecules, Biochem. Pharmacol. 182 (2020) 114211, https://doi.org/10.1016/j.bcp.2020.114211.

[54] W.C. Hon, M.I. Wilson, K. Harlos, T.D. Claridge, C.J. Schofield, C.W. Pugh, P. H. Maxwell, P.J. Ratcliffe, D.I. Stuart, E.Y. Jones, Structural basis for the recognition of hydroxyproline in HIF-1α by pVHL, Nature 417 (2002) 975–978, https://doi.org/10.1038/nature00767.

[55] J.S. Schneekloth, F.N. Fonseca Jr., M. Koldobskiy, A. Mandal, R. Deshaies, K. Sakamoto, C.M. Crews, Chemical genetic control of protein levels: selective in vivo targeted degradation, J. Am. Chem. Soc. 126 (2004) 3748–3754, https://doi.org/10.1021/ja039025z.

[56] M.S. Gadd, A. Testa, X. Lucas, K.H. Chan, W.Z. Chen, D.J. Lamont, M. Zengerle, A. Ciulli, Structural basis of PROTAC cooperative recognition for selective protein degradation, Nat. Chem. Biol. 13 (2017) 514–521.

[57] G.E. Winter, D.L. Buckley, J. Paulk, J.M. Roberts, A. Souza, S. Dhe-Paganon, J. E. Bradner, Structural basis of PROTAC cooperative recognition for selective protein degradation, Science 348 (2015) 1376–1381, https://doi.org/10.1038/nchembio.2329.

[58] O. Gulec, C. Turkes, M. Arslan, Y. Demir, B. Dincer, A. Ece, O.I. Kkufrevioglu, S. Beydemir, Bioactivity, cytotoxicity, and molecular modeling studies of novel sulfonamides as dual inhibitors of carbonic anhydrases and acetylcholinesterase, J. Mol. Liq. 410 (2024) 125558, https://doi.org/10.1016/j.molliq.2024.125558.

[59] O. Gulec, C. Turkes, M. Arslan, Y. Demir, B. Dincer, A. Ece, O.I. Kufrevioglu, S. Beydemir, Novel spiroindoline derivatives targeting aldose reductase against diabetic complications: bioactivity, cytotoxicity, and molecular modeling studies, Bioorg. Chem. 145 (2024) 107221, https://doi.org/10.1016/j.bioorg.2024.107221.

[60] Y. Demir, F.S. Tokalı, E. Kalay, C. Turkes, P. Tokali, O.N. Aslan, K. Sendil, S. Beydemir, Synthesis and characterization of novel acyl hydrazones derived from vanillin as potential aldose reductase inhibitors, Mol. Divers. 27 (2023) 1713–1733, https://doi.org/10.1007/s11030-022-10526-1.

[61] O. Gulec, C. Turkes, M. Arslan, Y. Demir, B. Dincer, A. Ece, S. Beydemir, Novel beta-lactam substituted benzenesulfonamides: in vitro enzyme inhibition, cytotoxic activity and in silico interactions, J. Biomol. Struct. Dyn. 42 (2023) 63559–66377, https://doi.org/10.1080/07391102.2023.2240889.

[62] F.S. Tokalı, Y. Demir, C. Türkeş, B. Dinçer, Ş. Beydemir, Novel acetic acid derivatives containing quinazolin-4(3H)-one ring: synthesis, in vitro, and in silico evaluation of potent aldose reductase inhibitors, Drug Dev. Res. 84 (2023) 275–295, https://doi.org/10.1002/ddr.22031.

[63] S.H. Dehkordi, S. Farhadian, M. Ghasemi, The interaction between the azo dye tartrazine and α-chymotrypsin enzyme: molecular dynamics simulation and multi-spectroscopic investigations, J. Mol. Liq. 344 (2021) 117931, https://doi.org/10.1016/j.molliq.2021.117931.

[64] F. Yazdani, B. Shareghi, S. Farhadian, L. Momeni, Structural insights into the binding behavior of flavonoids naringenin with human serum albumin, J. Mol. Liq. 349 (2022) 118431, https://doi.org/10.1016/j.molliq.2021.118431.

[65] N. Farajzadeh-Dehkordi, S. Farhadian, Z. Zahraei, S. Asgharzadeh, B. Shareghi, B. Shakerian, Insights into the binding interaction of reactive yellow 145 with human serum albumin from a biophysics point of view, J. Mol. Liq. 369 (2023) 120800, https://doi.org/10.1016/j.molliq.2022.120800.

[66] A. Buza, C. Turkes, M. Arslan, Y. Demir, B. Dincer, A.R. Nixha, S. Beydemir, Novel benzenesulfonamides containing a dual triazole moiety with selective carbonic anhydrase inhibition and anticancer activity, RSC Med. Chem. (2025), https://doi.org/10.1039/D4MD00617H.

[67] A. Becker, S. Kohfeld, A. Lader, L. Preu, T. Pies, K. Wieking, Y. Ferandin, M. Knockaert, L. Meijer, C. Kunick, Development of 5-benzylpaullones and paullone-9-carboxylic acid alkyl esters as selective inhibitors of mitochondrial malate dehydrogenase (mMDH), Eur. J. Med. Chem. 45 (2010) 335–342, https://doi.org/10.1016/j.ejmech.2009.10.018.

[68] A. Joshi, R. Gupta, B. Singh, D. Sharma, M. Singh, Effective inhibitory activity against MCF-7, A549 and HepG2 cancer cells by a phosphomolybdate based hybrid solid, Dalton Trans. 49 (2020) 7069–7077, https://doi.org/10.1039/D0DT01042A.

[69] C.W. Lewis, R.G. Taylor, P.M. Kubara, K. Marshall, L. Meijer, R.M. Golsteyn, A western blot assay to measure cyclin dependent kinase activity in cells or in vitro without the use of radioisotopes, FEBS Lett. 587 (2013) 3089–3095, https://doi.org/10.1016/j.febslet.2013.08.003.

[70] R. Gussio, D.W. Zaharevitz, C.F. McGrath, N. Pittabiraman, G.E. Kellog, C. Schultz, A. Link, C. Kunick, M. Leost, L. Meijer, E.A. Sausville, Structure-based design modifications of the paullone molecular scaffold for cyclin-dependent kinase inhibition, Anticancer Drug Des. 15 (2000) 53–66.

[71] X. Xie, T. Lemcke, R. Gussio, D.W. Zaharevitz, M. Leost, L. Meijer, C. Kunick, Epoxide-containing side chains enhance antiproliferative activity of paullones, Eur. J. Med. Chem. 40 (2005) 655–661, https://doi.org/10.1016/j.ejmech.2005.02.004.

[72] E. Wang, H. Sun, J. Wang, Z. Wang, H. Liu, J.Z.H. Zhang, T. Hou, End-point binding free energy calculation with MM/PBSA and MM/GBSA: strategies and applications in drug design, Chem. Rev. 119 (2019) 9478–9508, https://doi.org/10.1021/acs.chemrev.9b00055.